ELSEVIER

Available online at www.sciencedirect.com

SCIENCE DIRECT®

Microelectronic Engineering 75 (2004) 137–144

MICROELECTRONIC ENGINEERING

www.elsevier.com/locate/mee

Computer simulation of multifinger heterojunction bipolar transistor with self-heating and thermal coupling models

Kuen Yu Huang [a], Yiming Li [b,c,*], C.-P. Lee [a]

[a] *Department of Electronics Engineering, National Chiao Tung University, P.O. Box 25-178, Hsinchu 300, Taiwan*
[b] *Department of Computational Nanoelectronics, National Nano Device Laboratories, Hsinchu 300, Taiwan*
[c] *Microelectronics and Information Systems Research Center, National Chiao Tung University, Hsinchu 300, Taiwan*

Received 23 November 2003; received in revised form 4 March 2004; accepted 9 March 2004
Available online 27 March 2004

Abstract

In this paper, we simulate the nonlinearity of a multifinger heterojunction bipolar transistor (HBT) operated at radio frequency (RF). We directly solve the nonlinear differential equations of the HBT large-signal model with the electrical–thermal feedback equations in time domain using the waveform relaxation (WR) and monotone iterative (MI) methods. The temperature dependence of energy band gap (E_g), current gain, saturation current and thermal conductivity are also taken into consideration. With the developed simulator, the power-added efficiency (PAE), 1-dB compression point ($P_{1\text{-dB}}$) and output third-order intercept point (OIP3) of a three-finger HBT are calculated. Our results illustrate the effects of self-heating and thermal coupling among different fingers play important roles in the nonlinearity of the multifinger power transistors. Furthermore, the proposed method allows us to evaluate the thermal effects on linearity of the multifinger power transistors and perform optimum design for these devices.
© 2004 Elsevier B.V. All rights reserved.

Keywords: Nonlinearity; Self-heating; Intermodulation; Distortion; Multifinger; OIP3; IIP3; Power transistor; Thermal; HBT model; Simulation

1. Introduction

High power HBTs operated at microwave and millimeter-wave frequencies have been of great interest for the applications of wireless and fiber communications in recent years [1–5]. These transistors, used for power applications, usually have multiple fingers to spread the current and the dissipated heat. Therefore, the self-heating effect and thermal coupling effect among fingers become important issues for multifinger power transistors [6–11]. In addition, the linearity of HBTs is also attractive to the applications of microwave and millimeter-wave engineering [12–18]. It is known

* Corresponding author. Tel.: +886-930-330-766; fax: +886-3-5726639.
E-mail addresses: ymli@mail.nctu.edu.tw (Y. Li).

0167-9317/$ - see front matter © 2004 Elsevier B.V. All rights reserved.
doi:10.1016/j.mee.2004.03.083

that the performance of linearity for a transistor varies with its operation conditions. Because the electrical characteristics are temperature dependant, the thermal effects will significantly influence the linearity of the power transistor [19–22]. In our recent work [23], a time domain approach to the characterization of the two-tone intermodulation distortion has been proposed. The electrical large-signal circuit problems are solved efficiently by our method with utilizing the WR and MI methods. With this simulation technique, we can examine the variate of HBT linearity under different electrical bias conditions.

We first in this paper introduce the temperature dependant equations to some physical parameters of the Gummel–Poon model. A thermal model that describes the relation between power dissipation and junction temperature is adopted. By considering the models above, the thermal–electrical feedback equations for the power HBT are achieved. We then solve the nonlinear differential equations of the HBT large-signal model and the coupled electrical–thermal feedback equations in time domain by employing the WR and MI methods [23,24]. In the thermal–electrical feedback equations, the temperature dependencies for the thermal conductivity are also included in our simulation model. The proposed model and simulation is implemented and applied to investigate the power-added efficiency (PAE), 1-dB compression point ($P_{1\text{-dB}}$), output third-order intercept point (OIP3) and input third-order intercept point (IIP3) of a three-finger HBT. By comparing the devices' linearity with their own junction temperature and current density, our results clearly illustrate that the effects of self-heating and thermal coupling among different fingers play important roles in the nonlinear phenomena of the multifinger power transistors. Our method allows us to evaluate the thermal effects on linearity of the multifinger power transistors directly. The model and simulation technique studied here can be further included in CAD tool for performing an optimum design of these devices.

Subsequent sections of this paper are organized as follows. Section 2 introduces the model and characterization method. Section 3 is the results and discussion. Comparisons and analyses are also presented in this section in detail. Section 4 draws the conclusion.

2. Computational model for multifinger HBT

The electrical model of HBT considered in our simulation is based on the Gummel–Poon (GP) large signal model [23,25,26]. For thermal–electrical feedback mechanism, the temperature dependant equations of some physical parameters are introduced to the GP model:

$$E_g(T_J) = E_g(T_A) + \frac{E_a \cdot T_A^2}{T_A + E_b} + \frac{E_a \cdot T_J^2}{T_J + E_b}, \tag{1}$$

$$\mathrm{IS}(T_J) = \mathrm{IS} \cdot \left(\frac{T_J}{T_A}\right)^{\mathrm{XTI}} \cdot \exp\left[\left(\frac{E_g(T_A)}{k \cdot T_A}\right) - \left(\frac{E_g(T_J)}{k \cdot T_J}\right)\right], \tag{2}$$

$$\mathrm{ISE}(T_J) = \mathrm{ISE} \cdot \left(\frac{T_J}{T_A}\right)^{\frac{\mathrm{XTI}}{\mathrm{NE}} - \mathrm{XTB}} \cdot \exp\left[\left(\frac{E_g(T_A)}{\mathrm{NE} \cdot k \cdot T_A}\right) - \left(\frac{E_g(T_J)}{\mathrm{NE} \cdot k \cdot T_J}\right)\right], \tag{3}$$

$$\mathrm{ISC}(T_J) = \mathrm{ISC} \cdot \left(\frac{T_J}{T_A}\right)^{\frac{\mathrm{XTI}}{\mathrm{NC}} - \mathrm{XTB}} \cdot \exp\left[\left(\frac{E_g(T_A)}{\mathrm{NC} \cdot k \cdot T_A}\right) - \left(\frac{E_g(T_J)}{\mathrm{NC} \cdot k \cdot T_J}\right)\right], \tag{4}$$

$$\mathrm{BF}(T_J) = \mathrm{BF} \cdot \left(\frac{T_J}{T_A}\right)^{\mathrm{XTB}}, \tag{5}$$

$$\mathrm{BR}(T_J) = \mathrm{BR} \cdot \left(\frac{T_J}{T_A}\right)^{\mathrm{XTB}}, \tag{6}$$

where T_J and T_A are junction and ambient temperature, respectively. We note that for high powered devices T_A is the temperature on the back of the substrate. Above equations include the temperature dependance of energy band gap (E_g), saturation current (IS), collector and emitter

leakage current (ISC and ISE), and current gain (BF and BR).

On the other hand, the thermal model expresses the relation between the power dissipation and the junction temperature. The junction temperature with considering the temperature-dependent thermal conductivity for n-finger HBT is

$$\mathbf{T}_\mathrm{J} = T_\mathrm{A}\left\{1 - \frac{(\mathrm{BB}-1)}{T_\mathrm{A}}[\mathbf{R}_\mathrm{TH}\cdot\mathbf{P}_\mathrm{D}]\right\}^{-1/(\mathrm{BB}-1)} = \begin{bmatrix} T_{\mathrm{J}1} \\ T_{\mathrm{J}2} \\ \vdots \\ T_{\mathrm{J}n} \end{bmatrix}, \quad (7)$$

where $T_{\mathrm{J}n}$ is the junction temperature of nth finger [7,8]. $\mathbf{R}_\mathrm{TH}\cdot\mathbf{P}_\mathrm{D}$ is given by

$$\mathbf{R}_\mathrm{TH}\cdot\mathbf{P}_\mathrm{D} = \begin{bmatrix} R_{\mathrm{T}11} & R_{\mathrm{T}12} & \dots & R_{\mathrm{T}1n} \\ R_{\mathrm{T}21} & R_{\mathrm{T}22} & & R_{\mathrm{T}2n} \\ \vdots & & \ddots & \vdots \\ R_{\mathrm{T}n1} & R_{\mathrm{T}n2} & & R_{\mathrm{T}nn} \end{bmatrix} \cdot \begin{bmatrix} P_{\mathrm{D}1} \\ P_{\mathrm{D}2} \\ \vdots \\ P_{\mathrm{D}n} \end{bmatrix}. \quad (8)$$

Here $R_{\mathrm{T}nn}$ and $R_{\mathrm{T}nm}$ denote the self-heating thermal resistance of nth finger and the coupling thermal resistance which counts the coupled heat from mth finger to nth finger, respectively. Furthermore, the power dissipation of nth finger is denoted by $P_{\mathrm{D}n}$. We note here that in general the values of $\mathbf{R}_\mathrm{TH}$ must be computed in advance with the help of a three-dimensional thermal analysis (for example, a finite element simulation of the structures).

As shown in Fig. 1, we briefly outline the computational flowchart for the proposed simulation technique. We combine the electrical and thermal models above, and perform the electrical–thermal iteration loop. This simulation technique, shown in Fig. 1, consists of the following steps:

- Step 1. We set all parameters of the electrical and thermal models, DC input current, RF input power, and the ambient temperature T_A.
- Step 2. We initialize the junction temperature (set $T_\mathrm{J} = T_\mathrm{A}$).

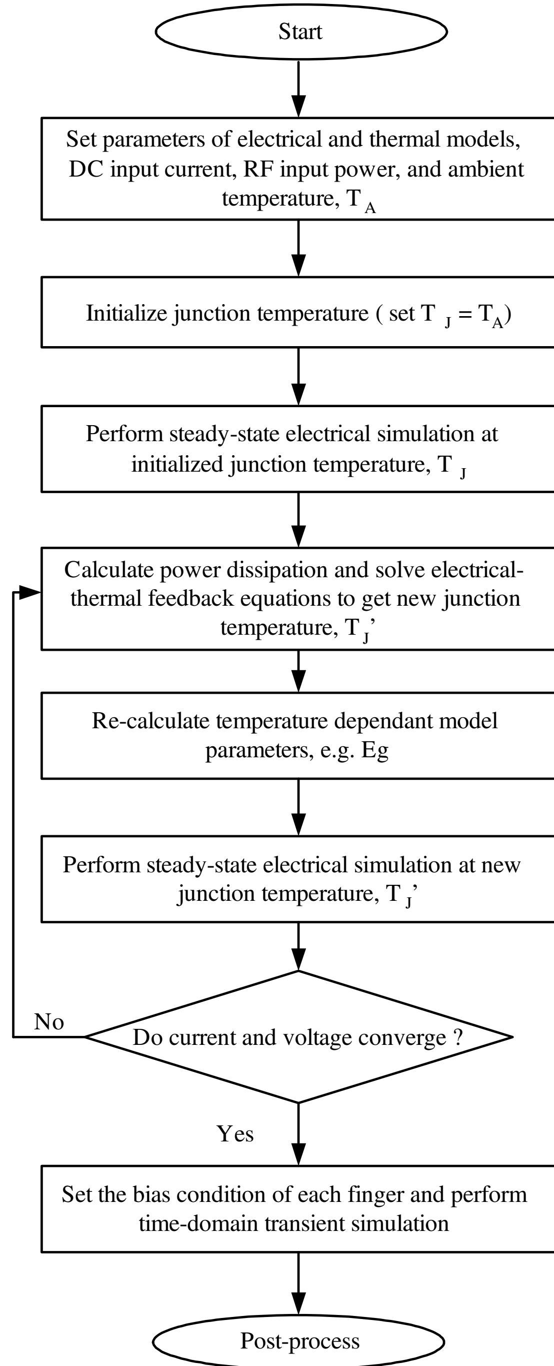

Fig. 1. A flowchart of the proposed simulation technique for the electrical–thermal feedback iteration.

- Step 3. The steady-state electrical simulation at initialized junction temperature T_J is performed.
- Step 4. Once the convergent results are obtained, we calculate the power dissipation and solve the electrical–thermal feedback equations to get new junction temperature T_J.
- Step 5. Temperature dependant model parameters, such as E_g will be then recalculated.
- Step 6. We perform the steady-state electrical simulation at this new junction temperature T_J.
- Step 7. Convergence test for all the calculated current and voltage will be performed. If all the computed physical quantities are convergent with a specified stopping criterion then Step (8) will be executed. Otherwise we return to Step (4) for next iteration; and
- Step 8. Set the bias condition of each finger and perform time-domain transient simulation.

The steady-state and time-domain transient simulation appeared above are accomplished by using the WR and MI techniques. Details of the simulation can be found in [23].

It is possible for all identical fingers to have different bias condition, due to the significance of the coupled electrical–thermal feedback. Therefore, this will influence the DC and RF characteristics of each finger and the whole multifinger transistor, in particular for devices under high current or high power operation. To clearly examine the nonlinearity, we perform the simulation for a three-finger HBT. Without loss of generality, each finger is theoretically assumed identical. The model parameters of the finger for both the electrical and thermal models are shown in Table 1. To validate these parameters, based on the DC and RF measurement, they are carefully calibrated, simulated, and extracted with a genetic algorithm [27].

An equivalent circuit of a tree-finger HBT is shown in Fig. 2. The Finger 1 of this HBT is represented by M1, and M2 and M3 are the Fingers 2 and 3, respectively. I_{BB} denotes the constant bias current at the base and P_{in} is the power of RF input signal. The behavior of Fingers 1 and 3 is the same for the identical fingers assumption. According to the case of the three-finger transistor, Eq. (7) is expressed as

Table 1
A set of the HBT parameters for the Gummel–Poon and thermal models

Notation	Value	Unit
IS	2.85E − 24	A
BF	86.95	–
NF	1.068	–
IKF	0.1815	A
IKR	1.032E − 3	A
ISE	2.34E − 18	A
NE	1.91	–
BR	1.47	–
NR	1.06	–
ISC	2.142E − 14	A
NC	1.954	–
RB	56.88	Ω
RE	10.256	Ω
RC	8.352	Ω
CJEO	130.0E − 15	F
VJE	1.367	V
XCJC	0.3428	–
VTF	66.0	V
ITF	419.80E − 3	A
TF	2.68E − 12	s
MJC	0.266	–
VJC	0.7161	V
CJCO	24.27E − 15	F
XTF	275.6	–
MJE	0.1188	–
TR	350.0E − 12	s
FC	0.5	–
E_a	5.405E − 4	eV/K
E_b	204	K
BB	1.22	–
XTI	3.0	–
XTB	−2.0	–

$$T_{J1} = T_{J3} = T_A \left\{ 1 - \frac{(\mathrm{BB} - 1)}{T_A} [P_{D1} \cdot (R_{TH0} + R_{TC2}) + P_{D2} \cdot R_{TC1}] \right\}^{-1/(\mathrm{BB}-1)}, \quad (9)$$

$$T_{J2} = T_A \left\{ 1 - \frac{(\mathrm{BB} - 1)}{T_A} [P_{D1} \cdot (2 \cdot R_{TC1}) + P_{D2} \cdot R_{TH0}] \right\}^{-1/(\mathrm{BB}-1)}, \quad (10)$$

where $R_{TH0} = R_{T11} = R_{T22} = R_{T33}$, $R_{TC1} = R_{T12} = R_{T21}$, and $R_{TC2} = R_{T13} = R_{T31}$. In our case, each finger has an emitter area of $2.8 \times 12\ \mu m^2$,and the substrate thickness is 100 μm. There is the same

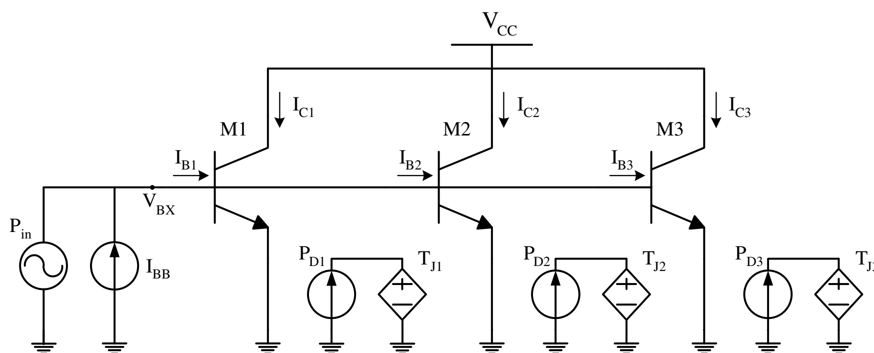

Fig. 2. An equivalent circuit of a three-finger HBT with constant current bias and RF input excitation.

spacing between Fingers 1 and 2, and between Fingers 2 and 3, which is 14.4 μm. Therefore, the theoretical values [7,8,26] of R_{TH0}, R_{TC1}, and R_{TC2} are 1834.20, 487.04, and 101.43 °C/W, respectively. Furthermore, the ambient temperature, T_A, is set to be 300 K and the energy band gap of GaAs at this temperature, $E_g(T_A)$, equals to 1.424 eV.

3. Results and discussion

The simulated common-emitter *I–V* characteristics of this three-finger HBT is shown in Figs. 3 and 4. Each line in these figures represents the collector current under constant input current bias (I_{BB}). Because of the self-heating effect, the total collector current decreases gradually as collector-

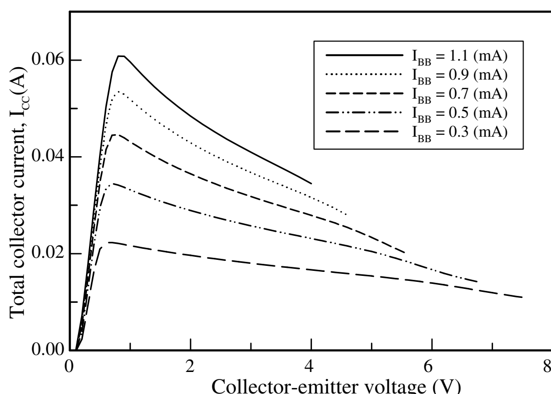

Fig. 3. The simulated common-emitter *I–V* characteristics for the whole three-finger HBT.

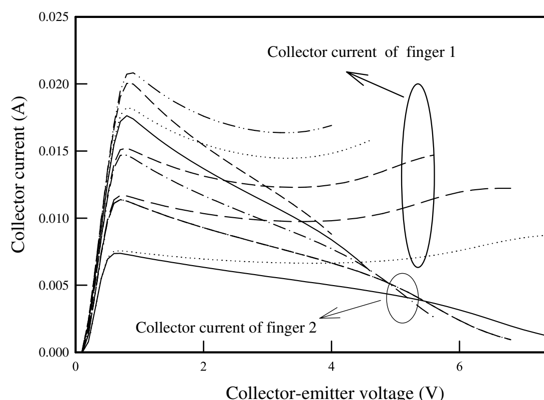

Fig. 4. The simulated common-emitter *I–V* characteristics for each finger of this HBT.

emitter voltage increases in Fig. 3. This situation results in a negative differential resistance region in the *I–V* characteristic and current gain collapse of this HBT. In Fig. 4, the collector current of central finger (Finger 2) decrease more serious than those of side finger (Finger 1), which is due to the coupled heat from two neighboring fingers. As the collector-emitter voltage increases even more ($V_{CC} > 4$ V), an abrupt lowering of the collector current of Finger 2 occurs. With the electrical–thermal iteration, our approach can explore the collapse phenomenon of the multifinger HBT under high voltage and high current bias.

Fig. 5 demonstrates the output power (P_{OUT}), power-added efficiency (PAE), and power gain for different values of input power (P_{in}). The input excitation is a single tone signal at 1.8 GHz. The

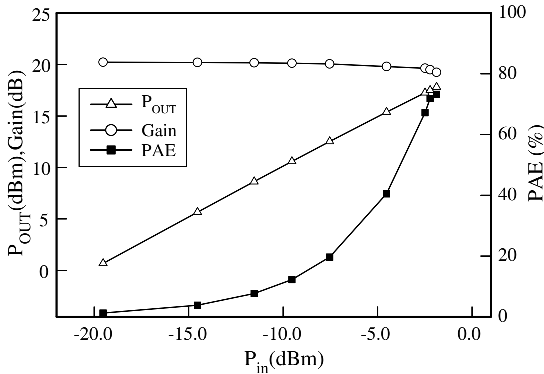

Fig. 5. The plots of output power, PAE, and the power gain versus the input power.

bias condition of this single tone simulation is with $V_{CC} = 3.6$ V and $I_{BB} = 0.6$ mA. In this simulation, we have taken the heating effect of input RF signal into consideration. It is found that, shown in Fig. 5, the power gain and PAE degrade as P_{in} increases, and 1-dB compression point ($P_{1\text{-dB}}$) is -2.45 dBm. The thermal coupling effect among fingers also influenced the performance of this three-finger device. As shown in Fig. 6, the PAE of central finger (Finger 2) is lower and degrades when $P_{in} > -3$ dBm. In the meanwhile, the PAE of the side finger (Finger 1) still rises as P_{in} increases. This phenomenon illustrates that the performance degradation of the whole transistor is mainly caused by the hotter central finger.

For two-tone intermodulation simulation, we perform four testing cases in this paper. Each case uses the same model parameters (as shown in Table 1), V_{CC} bias (3.6 V) and a two-tone excitation input. The input power of each tone is -10 dBm and the frequencies of this two-tone signal are 1.71 and 1.89 GHz, respectively. In the case A, we ignore all thermal effects, in other words, $R_{TH0} = R_{TC1} = R_{TC2} = 0$ °C/W. Only the self-heating effect is included in the case B, which means $R_{TC1} = R_{TC2} = 0$ °C/W and $R_{TH0} = 1834.20$ °C/W. For the case C, we consider both the self-heating and thermal coupling effects, and the values of thermal resistance R_{TH0}, R_{TC1}, and R_{TC2} are 1834.20, 487.04, and 101.43 °C/W, respectively. Finally, the case D has the same conditions as the case C, besides the consideration for heating effect of input RF signal. To incorporate the heating from the input signal for the case D, the averaged additional power is iteratively calculated with (9) and (10) until the junction temperature $\mathbf{T}_J$ converged.

The collector current density (J_{CC}) and junction temperature (T_J) of each finger in all cases are shown in Figs. 7 and 8, respectively. In the case A, T_J keeps a constant value (300 K) and J_{CC} rises almost linearly as I_{BB} increases since the thermal effects are ignored. It is found that, in the case B, there are suddenly jump for J_{CC} and T_J when $I_{BB} > 0.9$ mA. Furthermore, both J_{CC} and T_J of Finger 2 are higher than those of Finger 1 in the

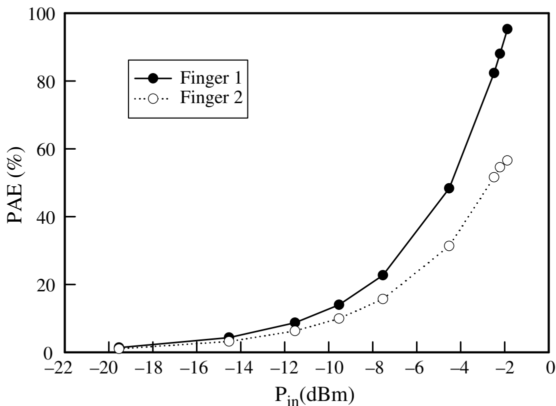

Fig. 6. Plots of PAE for Fingers 1 and 2 versus the input power.

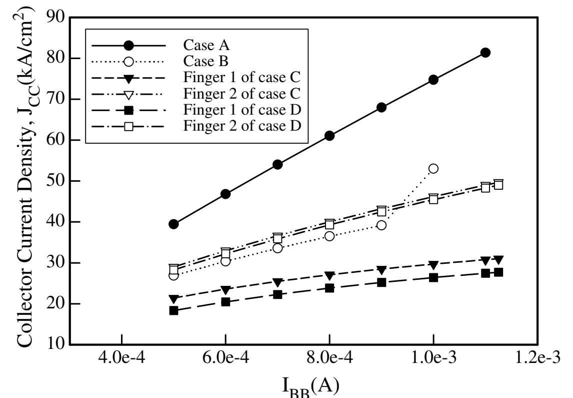

Fig. 7. Plots of collector current density (J_{CC}) versus input bias current (I_{BB}) for the cases A, B, C and D.

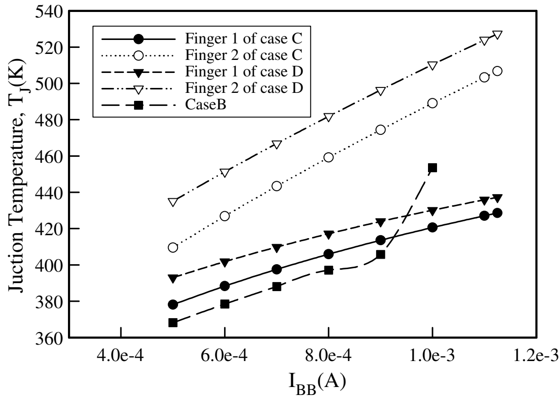

Fig. 8. Plots of the junction temperature (T_J) versus I_{BB} for the cases B, C, and D.

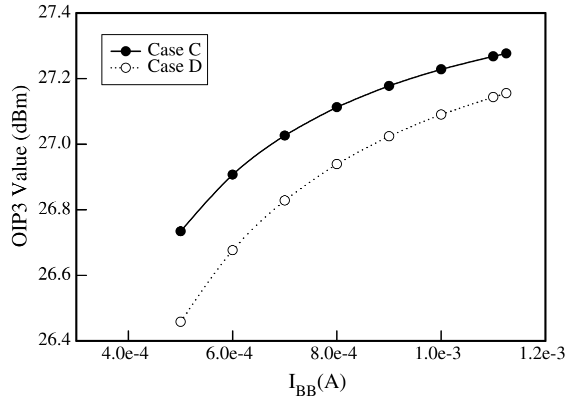

Fig. 10. A comparison of OIP3 values under different bias I_{BB} between the cases C and D.

cases C and D. Because of the consideration for additional heating from the RF input signal, T_J in the case D is higher than that in the case C, and J_{CC} in the case D is contrastively lower.

Fig. 9 shows the plots of OIP3 values versus I_{BB} for the testing cases A and B. OIP3 values of the case A are higher than those of the case B for the neglect of thermal effects in the case A. As $I_{BB} > 0.9$ mA, the OIP3 value begins to drop, and J_{CC} and T_J rise abruptly in the meantime. The self-heating effect downgrades the two-tone linearity of HBT in the case B. We take the thermal coupling effect among fingers into account in the cases C and D. It is found that, as shown in Fig. 10, OIP3 value varies smoothly with I_{BB}. Because there are two cold fingers (Fingers 1 and 3) in the cases C and D, the abrupt degradation for linearity in the case B can be prevented. In comparison between the cases C and D, OIP3 values in the case D are slightly lower than those in the case C for additional heating induced by the input RF signal. Furthermore, we demonstrate the input third-order intercept point (IIP3) values for each finger in Fig. 11. It is reasonable that the colder finger (Finger 1) has better linearity. In comparison with the case C, the difference in linearity performance between fingers for the case D is enlarged by the additional heating. This expansion of difference among fingers lowers the OIP3 values of whole device as shown in Fig. 10.

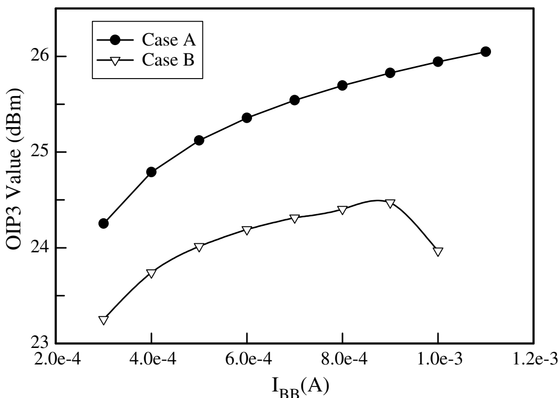

Fig. 9. A comparison of OIP3 values under different bias I_{BB} between the cases A and B.

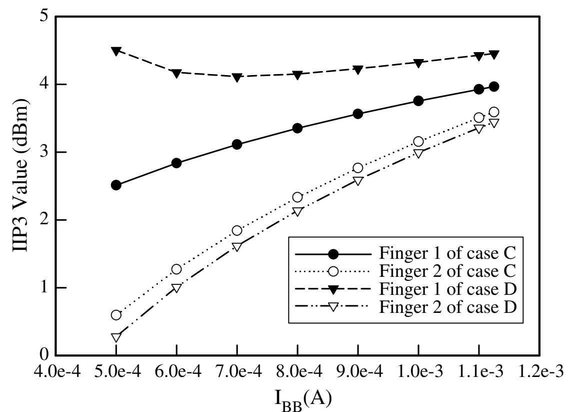

Fig. 11. Polts of the input third-order intercept point (IIP3) values versus I_{BB} for the cases C and D.

4. Conclusions

The nonlinearity of the RF multifinger HBT has been numerically investigated in this paper. The nonlinear differential equations of the HBT large-signal model with the electrical–thermal feedback equations in time domain have been successfully solved with the WR and MI methods. In the model, the temperature dependence of energy band gap, current gain, saturation current, and thermal conductivity have been included and evaluated. Simulation results of different testing conditions show the thermal effects on the linearity of the power HBT. Several benchmarks of the linearity for a three finger RF HBT have also been characterized. The nonlinear influence of the self-heating effect and the thermal coupling among fingers have been determined by comparing the linearity variation of the device with its own junction temperature and current density. Achieved results have confirmed that it is possible to directly evaluate the thermal effects on linearity of the multifinger power transistors with our simulation technique. The modeling and simulation discussed here can be further included in a CAD tool for performing optimum device design and circuit simulation.

Acknowledgements

The authors express their appreciation to the referees for a painstaking reading of the manuscript and for valuable suggestions. This work is supported in part by the National Science Council (NSC) of TAIWAN under Contract Nos.: NSC-90-2215-E009-056, NSC-92-2112-M-429-001 and NSC-92-2815-C-492-001-E. It is also supported in part by the grant of the Ministry of Economic Affairs, Taiwan under Contract No. 92-EC-17-A-07-S1-0011.

References

[1] B. Bayraktaroglu, J.A. Higgins, HBTs for microwave power applications, in: M.F. Chang (Ed.), Current Trends in Heterojunction Bipolar Transistors, World Scientific, Singapore, 1996.
[2] M. Yanagihara, H. Sakai, Y. Ota, A. Tamura, Solid-State Electron. 41 (1997) 1615–1620.
[3] N. Pan, J. Elliott, M. Knowles, D.P. Vu, K. Kishimoto, J.K. Twynam, H. Sato, M.T. Fresina, G.E. Stillman, IEEE Trans. Electron. Dev. 19 (April) (1998) 115–117.
[4] Y.S. Lee, C.S. Park, Proc. IEEE RAWCON (2001) 249–252.
[5] T. Oka, K. Hirata, H. Suzuki, K. Ouchi, H. Uchiyama, T. Taniguchi, K. Mochizuki, T. Nakamura, IEEE Trans. Electron. Dev. 48 (November) (2001) 2625–2630.
[6] W. Liu, Jpn. J. Appl. Phys. 32 (1993) 5503–5507.
[7] C.H. Liao, C.P. Lee, IEEE Trans. Electron. Dev. 49 (May) (2002) 909–915.
[8] L.L. Liou, J.L. Ebel, C.I. Huang, IEEE Trans. Electron. Dev. 40 (January) (1993) 35–43.
[9] J.J. Liou, L.L. Liou, C.I. Huang, IEE Proc. Circuits, Dev. Syst. 141 (December) (1994) 469–475.
[10] Y. Zhu, J.K. Twynam, M. Yagura, M. Hasegawa, T. Hasegawa, Y. Eguchi, Y. Amano, E. Suematsu, K. Sakuno, N. Matsumoto, H. Sato, N. Hashizume, IEEE Trans. Electron. Dev. 48 (November) (2001) 2640–2646.
[11] S. Heckmann, R. Sommet, J.-M. Nebus, J.-C. Jacquet, D. Floriot, P. Auxemery, R. Quere, IEEE Trans. Microwave Theory Tech. 50 (December) (2002) 2811–2819.
[12] B. Li, S. Prasad, IEEE Trans. Microwave Theory Tech. 45 (July) (1997) 1135–1137.
[13] B. Troyanovsky, Z. Yu, R.W. Dutton, Comput. Methods Appl. Mech. Eng. 181 (2000) 467–482.
[14] J. Lee, W. Kim, Y. Kim, T. Rho, B. Kim, IEEE Trans. Microwave Theory Tech. 45 (December) (1997) 2065–2072.
[15] B. Li, S. Prasad, IEEE Trans. Microwave Theory Tech. 46 (September) (1998) 1321–1323.
[16] M. Iwamoto et al., IEEE Trans. Microwave Theory Tech. 48 (December) (2000) 2377–2388.
[17] G. Niu, Q. Liang, J.D. Cressler, C.S. Webster, D.L. Harame, IEEE RFIC Symp. Dig. (2001) 147–150.
[18] Y. Wang, S.V. Cherepko, J.C.M. Hwang, F. Wang, W.D. Jemison, IEEE GaAs IC Symp. Tech. Dig. (2001) 20–204.
[19] P.M. Asbeck, H. Kobayashi, M. Iwamoto, G. Hanington, S. Nam, L.E. Larson, IEEE MTT-S Microwave Symp. Dig. (2002) 135–138.
[20] Y. Zhu, Q. Cai, R. Balasubramanian, J. Gerber, Proc. IEEE RAWCON (2001) 129–132.
[21] A. Samelis, D. Pavlidis, IEEE Trans. Microwave Theory Tech. 45 (April) (1997) 534–542.
[22] H.-M. Park, S. Hong, IEEE Trans. Electron. Dev. 49 (December) (2002) 2099–2106.
[23] K.Y. Huang, Y. Li, C.P. Lee, IEEE Trans. Microwave Theory Tech. 51 (October) (2003) 2055–2062.
[24] Y. Li, WSEAS Trans. Mathematics 1 (2002) 159–164.
[25] L.E. Getreu, Modeling the Bipolar Transistor, Elsevier, Amsterdam, 1984.
[26] W. Liu, Handbook of III–V Heterojunction Bipolar Transistor, Wiley, New York, 1998.
[27] Y. Li, Y.-Y. Cho, C.-S. Wang, K.Y. Huang, Jpn. J. Appl. Phys. 42 (April) (2003) 2371–2374.